

NASA Technical Memorandum 106487

# Interface Shape and Convection During Solidification and Melting of Succinonitrile

Henry C. de Groh III  
*Lewis Research Center*  
*Cleveland, Ohio*

and

Tiffany Lindstrom  
*University of Arizona*  
*Tucson, Arizona*

June 1994



National Aeronautics and  
Space Administration

# Interface Shape and Convection During Solidification and Melting of Succinonitrile

Henry C. de Groh III  
National Aeronautics and Space Administration  
Lewis Research Center  
Cleveland, Ohio 44135

Tiffany Lindstrom  
University of Arizona  
Department of Materials Science and Engineering  
Tucson, Arizona 85721

## ABSTRACT

An experimental study was conducted of the crystal growth of succinonitrile during solidification, melting and no-growth conditions using a horizontal Bridgman furnace and square glass ampoule. For use as input boundary conditions to numerical codes, thermal profiles on the outside of the ampoule at five locations around its periphery were measured along the ampoule's length. Temperatures inside the ampoule were also measured. The shapes of the s/l interface in various two-dimensional planes were quantitatively determined. Though interfaces were nondendritic and noncellular, they were not flat, but were highly curved and symmetric in only one unique longitudinal y-z plane (at  $x = 0$ ). The shapes of the interface were dominated by the primary longitudinal flow cell characteristic of shallow cavity flow in horizontal Bridgman; this flow cell was driven by the imposed furnace temperature gradient and caused a "radial" thermal gradient such that the upper half of the ampoule was hotter than the bottom half. We believe that due to the strong convection, the release of latent heat does not significantly influence the thermal conditions near the interface. We hope that the interface shape and thermal data presented in this paper can be used to optimize crystal growth processes and validate numerical models.

## INTRODUCTION

Crystal quality is an important factor in the manufacture of electronic materials, and other products, and is usually characterized by dislocation density and solute segregation. It has been shown that convection can influence the shape of the solid/liquid (s/l) interface, radial and longitudinal segregation, and other aspects of the solidification process.<sup>1-5</sup> However, a quantitative understanding and analysis of the interplay among convection, interface shape, and segregation is still lacking. The objective of this work was to determine quantitatively the shape of a s/l interface during solidification, melting, and no growth conditions in a horizontal Bridgman furnace. This information will be used to develop and test a numerical code capable of predicting the shape of the interface, convective flow velocity, and solute and temperature profiles.

The two basic forms of segregation which present a significant problem during crystal growth are end-to-end macrosegregation and radial segregation. Strong convective flows enrich the far field liquid with solute causing end to end macrosegregation, whereas radial segregation can be caused by high and low levels of convective flow or curved s/l growth interfaces. Radial segregation can be minimized with the use of strong forced convection at the s/l interface (as done in

Czochralski growth), but end-to-end segregation is generally still a problem. This paper deals with the relationship among convection, interface shape, and imposed temperature profiles. We hope that developing knowledge of the s/l interface shape during solidification will help optimize crystal growth processes and quality.

The horizontal Bridgman technique is widely used for research of electronic materials and heat transfer.<sup>6-8</sup> During horizontal Bridgman growth, convective flows have been shown to be strong and produce “shallow cavity flow.” Convection in a vertical orientation is generally reported to be “axisymmetric flow.”<sup>4</sup> Axisymmetric flow is generally much weaker than the shallow cavity flow present in the horizontal orientation, but axisymmetric flow is still responsible for poor radial homogeneity and can also contribute to longitudinal segregation. It has been proposed that the low-g environment of space be used for crystal growth to drastically reduce levels of convection and segregation; however, the orientation of residual gravity vectors during space processing are not always known or controllable. In addition, the relationship among gravity orientation, convection, and segregation is not well understood. Xu et al. have numerically studied the effects of gravity orientation in 2-dimensions in a simplified crystal growth arrangement.<sup>9</sup> In order to further understand the effects of gravity our ongoing research will examine how different gravity levels and orientations influence different aspects of Bridgman crystal growth, such as interface shape, on earth and in space.

Inatomi et al. have studied convective mixing and the rate of directional solidification in succinonitrile (SCN).<sup>10</sup> The effects of thermal convection on a nongrowing, stationary interface have also been previously studied.<sup>3,11</sup> Previous experiments showed that bulk motion in the liquid, specifically thermal convection, deformed the s/l interface into a complex curved shape.<sup>11</sup> Good agreement was achieved among these experiments and a 2-dimensional finite element model based on FIDAP<sup>12</sup> and a 3-dimensional finite difference model. In those experiments the furnace remained stationary<sup>3,11</sup> (no-growth). In the experiments presented here, the furnace was moved at a constant rate to induce solidification (and melting), and the resulting interface shapes and temperature measurements were compared to those from the no-growth situation.

## EXPERIMENTAL PROCEDURE

Experiments were performed in a manner similar to those previously discussed.<sup>3,11</sup> A Bridgman type furnace employing two copper jackets 0.5 cm apart, each with its own constant temperature bath, was used. The experiments were conducted with the furnace in a horizontal orientation, at furnace translation rates of 0  $\mu\text{m/s}$  (no growth), 40  $\mu\text{m/s}$  (solidifying), and -40  $\mu\text{m/s}$  (melting). The heating and cooling jackets have a 1.1 cm square hole into which the ampoule fits. The borosilicate glass ampoules have a 0.8 cm outer square cross section and are 15 cm long with a wall thickness of approximately 0.1 cm. A schematic of the furnace system is shown in Figure 1.

The ampoules were filled under vacuum with succinonitrile (SCN); the properties of the glass and SCN are listed in Table 1. The SCN used was purified,<sup>13</sup> thus, eliminating solutal convection. A microscope and camera were used to examine the s/l interface. Figure 2 shows the right-hand-rule coordinate system used; the origin (0,0,0) was defined as the center of the ampoule cross section and mid-way between the hot and cold zones. The interfaces were analyzed at the mid-center vertical plane of the ampoule (MCP), top-center horizontal plane of the ampoule (TCP) and the top wall, or top inner surface of the ampoule (TW). In some cases the interface

was also quantified where it contacts the front vertical wall (FW) of the ampoule. The MCP corresponds to the  $(0,y,z)$  plane (the  $y-z$  plane at  $x = 0$ ). TCP is the interface shape in the  $x-z$  plane at  $y = 1.5$  mm for the no-growth case,  $y = 1.0$  mm during solidification, and  $y = 2.5$  mm for the melting case. TW is the  $(x,3\text{ mm},z)$  plane, and FW is in the plane  $(3,y,z)$ . These interface shapes will be quantitatively compared to numerical simulations in a later paper.

In all experiments, no-growth (SCN4), solidification (SCN8), and melting (SCN9), the heating and cooling jackets were maintained at a temperature difference of  $63\text{ }^\circ\text{C} \pm 1^\circ\text{C}$  with a hot zone temperature of  $78\text{ }^\circ\text{C}$  for no-growth and  $75\text{ }^\circ\text{C}$  during solidification and melting. The resulting temperatures on the outside surface of the ampoule were measured with type K thermocouples attached to the top, bottom, front, and corners of the ampoule as shown in Figure 2. In the no-growth case, temperature was also measured along the center of the ampoule  $(0,0,z)$  and along  $(0,1.54\text{mm},z)$ . Temperature measurements were taken every 1 to 2 mm. The resulting temperature profiles on the outside of the ampoule at the front wall are shown in Figure 3.

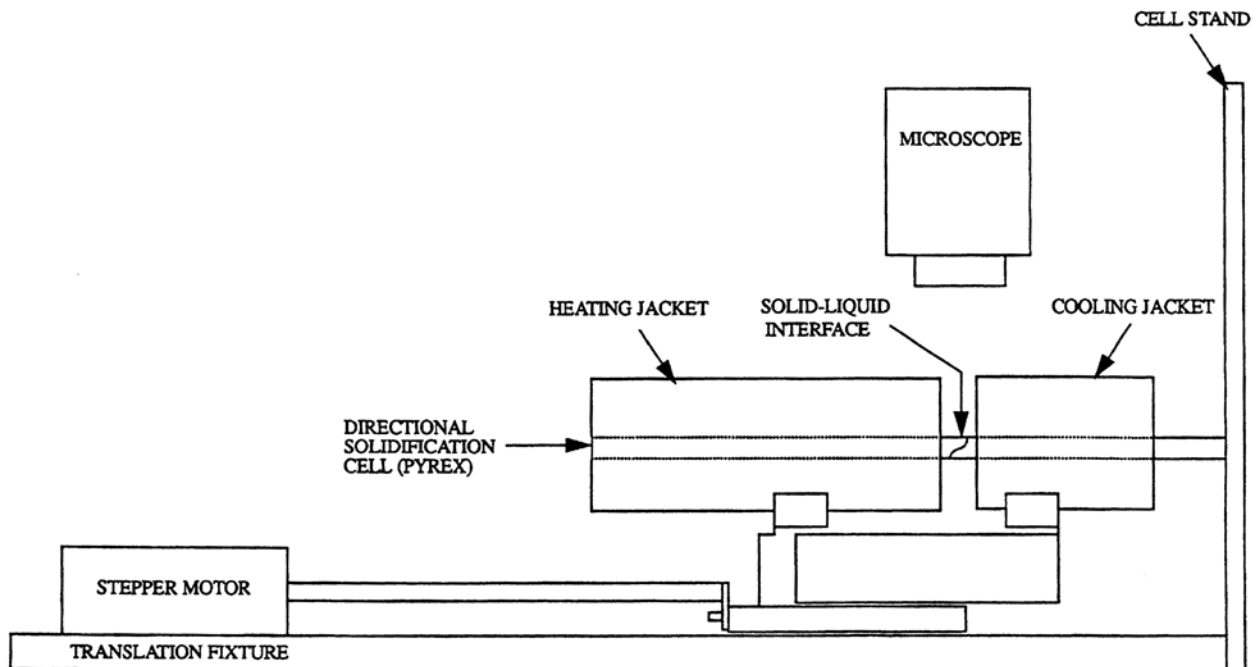


Figure 1. Schematic of the apparatus with microscope above;  $z = 0$  is at the center of the gap between the cooling and heating jackets.

Table 1. Properties of succinonitrile and borosilicate glass ampoules.<sup>13-15</sup>

Property	SCN-liquid	SCN-solid	SCN-interface	Ampoule
Density, $\rho$ , $\text{kg/m}^3$	984.	1016		2300.
Thermal conductivity, $\kappa$ , $\text{W/m-K}$	0.223	0.225		1.2
Heat capacity, $C_p$ , $\text{J/kg-K}$	2000.	1955		753.5
Thermal expansivity, $\beta$ , $\text{K}^{-1}$	$8.1 \times 10^{-4}$			
Kinematic viscosity, $\nu$ , $\text{m}^2/\text{s}$	$2.6 \times 10^{-6}$			
Melting temperature, $T_m$ , $\text{K}$			331.34	

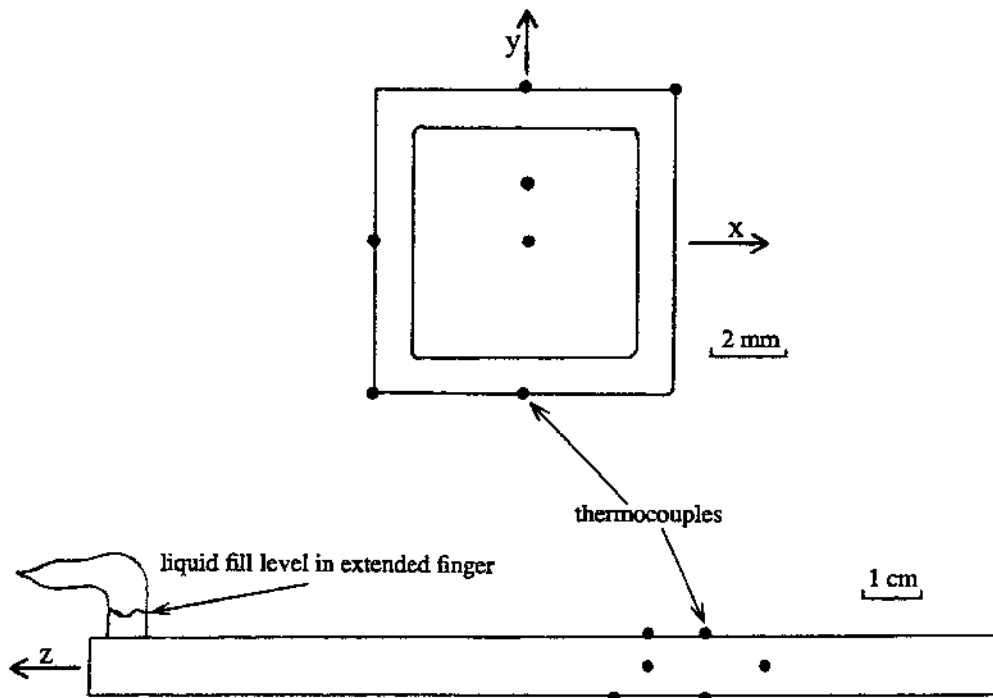


Figure 2. Sketch of the ampoule and thermocouple locations, showing cross section and side views and the right-hand-rule coordinate system used.

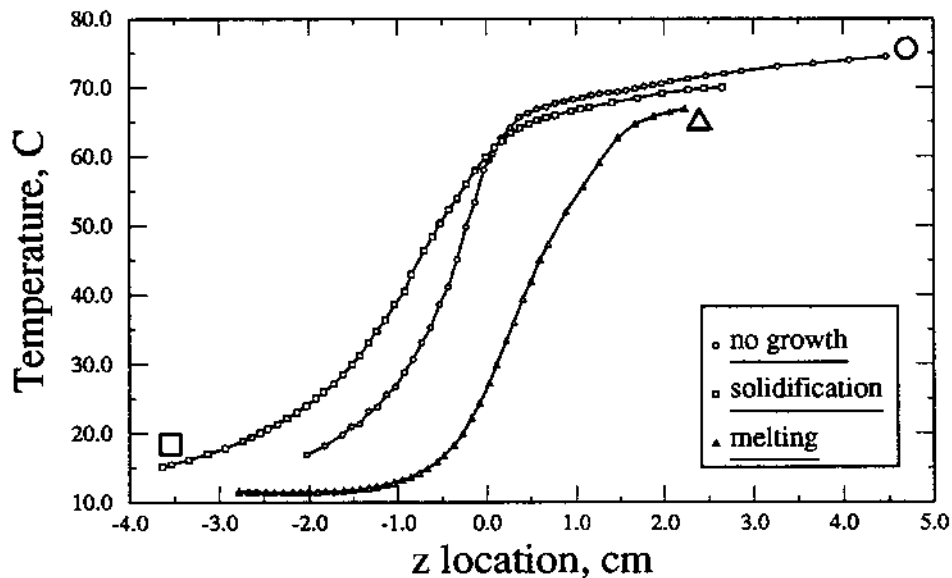


Figure 3. Temperature profile along the outside of the ampoule at the front wall during no-growth, solidification and melting experiments.

Photographs were taken of the interface at what were observed to be steady state conditions. The system required about 10 minutes to equilibrate and achieve a steady state; only then were photographs taken. The photographs were then digitized. The shape of the interface and its approximate location were determined from the photographs and its location adjusted using the temperature/distance measurements. Since the thermal gradient through the ampoule was found

to be nearly zero, the interface position could be determined from the location of the surface thermocouple when it indicated the melting temperature.

Experimental errors make agreement between the numerical codes and experiments quite difficult. There is an error of approximately  $\pm 0.5$  mm in the z-axis location of the interface taken from photographs. There is also an error of a maximum of  $\pm 0.5$  mm in the location of the thermocouple beads, which are also used to determine the location of the interface shapes. Although thermocouple accuracy is very high at the low temperatures used in this study, the thermocouple error was estimated to be  $\pm 1$  °C; due primarily to the presence of the glue used to bond the thermocouple to the glass. These uncertainties often cause problems with the consistency of the measured thermocouple data and interface positions. To minimize the uncertainties, a simple averaging method was established to make the experiment data more consistent. This method incorporates the information from thermocouple data, the side-view (mid-center plane) photographs and the top-view (top wall) photographs of the interface. Point locations (z-locations) are found using the temperature data, where  $T = 58$  °C, the melting temperature of SCN. These z-locations are also found by locating the interface, relative to the center of the gap, in the photograph. In general, when the data are merged to make them consistent, each data set is moved one half the difference between them. For example, set “a” is moved towards set “b”, and then “b” is moved towards set “a”. This makes for a more consistent set of data points, and a better set of input boundary conditions to numerical codes. Interface data in the x-z plane are averaged so that those interfaces are symmetrical.

## RESULTS

The thermal profiles measured along the length of the ampoule for the three cases (no-growth, solidification, and melting) are given in Appendix Tables A1, A2, and A3; these will be used in a later paper as input thermal boundary conditions. The temperature measurements made inside the ampoule ( $T_c$  and  $T_{ui}$ , in Table A1) will not be used as boundary conditions but we hope will provide a valuable comparison to the results of the numerical simulations. The thermal data for the center of the vertical face of the ampoule (3mm,0,z) are shown in Figure 3.

The interface shapes observed during the experiments are shown in Figures 4 through 10. The interface shape data are given in Appendix Tables A4 through A13.

### *No-Growth*

The interface at the mid-center plane (MCP) which resulted during the no-growth case, shown in Figures 5 and 10, was been previously determined.<sup>3,11,16</sup> Figures 4 and 5 show the interface shape in the top-center-plane (x,1.5mm,z) and where the interface meets the top wall and the front wall. As viewed from the liquid, the solid is concave; the solid and liquid fit together such that the solid is female and the liquid is male. The solid appears to be convex at the upper portion of the front wall (3,2.5,0.6); however, this is deceptive because the shape is at the ampoule border and the corners of the ampoule are rounded (not ideally square). The front wall interface is not similarly curved at the bottom because the interface along the bottom wall is flat. The flat, linear nature of the interface at the bottom wall (x,-3,z) during no-growth was discernible during experiments, but could not be documented quantitatively. The maximum deflection of the MCP interface, described by the difference between the maximum and minimum z locations of the interface, was 3.5 mm. The maximum z-axis deflection of the interface in the TCP was 1.3 mm.

The thermal convection in the liquid, driven by the longitudinal temperature gradient, is believed responsible for the concavity of the solid and its asymmetry, shown in Figure 5. Flow in the liquid was observed and approximate velocities near the interface in the range of 0.4 to 1.6 mm/s measured.<sup>11</sup> In the  $y$ - $z$  plane a strong recirculating flow cell was observed with a vortex at approximately  $(0,1,1.5)$ . Previous (and ongoing) numerical simulations have determined the flow to be a complex 3-dimensional flow known as “shallow cavity” flow.<sup>4</sup> The flow observed is

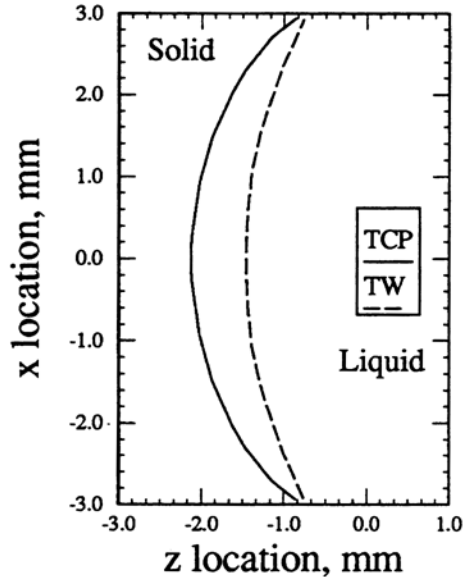


Figure 4. Top view of the interface during the no-growth experiment, top-center-plane  $(x,1.5,z)$  TCP and at the top wall of the ampoule  $(x,3,z)$  TW.

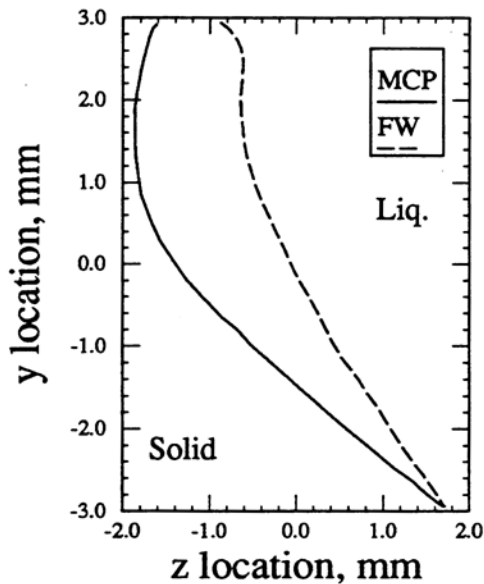


Figure 5. Side view of interface (mid-center-plane  $(0,y,z)$  and front wall  $(3,y,z)$ ) during no-growth experiment.

consistent with the shallow cavity flow model and can be described as follows for the no-growth case: in the  $y$ - $z$  plane, a single recirculating flow cell brings hot liquid along the top wall, raising and homogenizing the top wall temperature and ramming hot liquid against the upper portion of the interface. The liquid turns downward when confronted by the interface, is cooled by the interface and imposed thermal gradient, and returns along the bottom wall of the ampoule. Our numerical simulations<sup>11,17</sup> indicate that in the  $x$ - $y$  plane a four-cell flow pattern is also present; two counterrotating cells in the upper portion of the ampoule ( $y > 0$ ) in which the flow moves down along the vertical walls and up from the center, and two counterrotating cells in the lower portion ( $y < 0$ ) with liquid moving up along the vertical walls and down in the center. The relative magnitudes of these flows result in a complex flow structure that varies along the length of the ampoule. The details of these flows will be dealt with in a later paper.

### *Solidification*

The interface shapes that were observed in various planes during solidification are shown in Figures 6, 7, and 10. The solidification interface data are given in Appendix Tables A8, A9, and A10. The no-growth and solidification interface shapes are similar, however, the shape formed during solidification was more curved, with the liquid reaching further into the solid. The maximum  $z$ -axis deflection in the MCP was 7.2 mm, compared to 3.5 mm during no-growth. Maximum  $z$  deflection in the TCP ( $x, l, z$ ) was 3.0 mm, compared to 1.3 during no-growth ( $x, l, z$ ). The interface shape at the front wall could not be quantitatively determined for the solidification and melting cases, thus is not given in Figures 7 and 9.

We believe that the interface shape is dominated by the heat transferred by the convecting liquid and conduction through the solid, and that the release of latent heat has little influence on the thermal conditions in the neighborhood of the interface. Warmer liquid from the inner regions of the hot zone is continually convecting upon the upper half of the solid. As the cool zone moves toward the liquid, the solid in contact with the ampoule is brought along with it; however, the inner regions of the solid must conduct the heat through the relatively low conducting SCN. As a result, a “radial” temperature gradient (larger than in the no-growth case) develops. In a later paper we will examine, using numerical simulations, the influence of latent heat on the interface shape, as well as other aspects of solidification.

We believe the flow present during solidification to be shallow cavity flow. Though a quantitative determination of flow velocities was beyond the scope of the present work, maximum flow velocities are expected to be similar to those measured previously and in the range of 1 to 2 mm/s.<sup>11</sup>

### *Melting*

The interface shapes found during melting are shown in Figures 8, 9, and 10. When viewed from the liquid side, the MCP interface was concave in the upper half of the ampoule ( $y > 0$ ), and convex in the lower portion ( $y < 0$ ). During melting the solid is being moved toward the hot zone and the solid is encouraged to melt from the outside in towards the center. Thus the interface shape is encouraged to be convex, and is in the bottom half. However, in the horizontal orientation, heat transfer due to convection still manages to dominate in the upper half of the MCP interface, causing it to be concave for positive  $y$ . The natural convection causes a large thermal gradient along the vertical  $y$ -axis because the light, warm liquid moves along the top wall, with the cooler, heavier liquid returning along the bottom wall. Thus the maximum  $z$ -deflection of the

MCP, 3.7 mm, remains about the same as compared to the no-growth case. Shallow cavity flow is not expected to induce significant thermal gradients along the x-axis; however, due to the side walls, the flow striking the upper center of the interface ( $0, y > 0, z$ ) is more intense than at the side walls. Thus there is still a concave z-deflection of the TCP ( $x, 2.5, z$ ) during melting, 0.8 mm, though it is much less than during no-growth, 1.3 mm, or solidification, 3 mm.

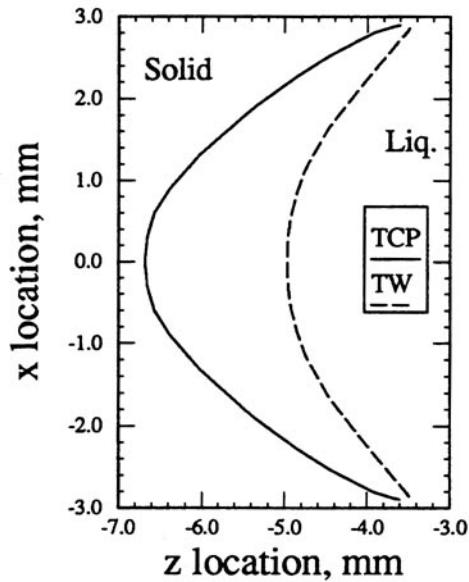


Figure 6. Top view of interface during solidification, top-center plane ( $x, 1, z$ ) and at the top wall of the ampoule ( $x, 3, z$ ).

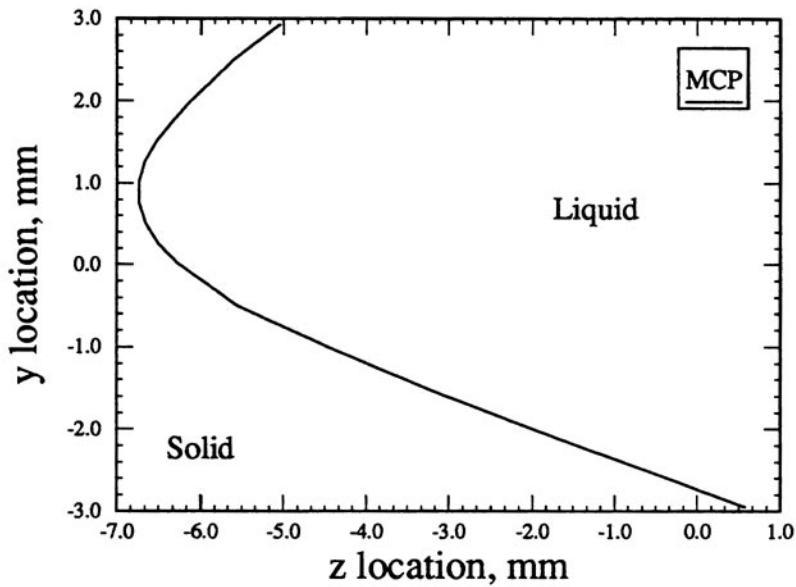


Figure 7. Side view of the interface ( $0, y, z$ ) during solidification experiment.

Figure 10 shows the location and shape of the interfaces in the MCP for the three cases examined. During no-growth the entire interface can be observed in the 5 mm gap between the hot and cool zones. When the furnace system is moved toward the hot zone (+ z direction) to induce solidification, the interface moves partially into the cool zone. When the furnace is reversed, during melting, solid and the interface are forced into the hot zone. These interface locations were achieved using approximately the same thermal gradient and furnace set point temperatures. An important part of the art and science of solidification is the modification of the interface shape through manipulation of 1) thermal gradient, and 2) at constant gradient, furnace set points. We hope the numerical codes<sup>11,12,16</sup> will help to quantify and optimize this aspect of crystal growth.

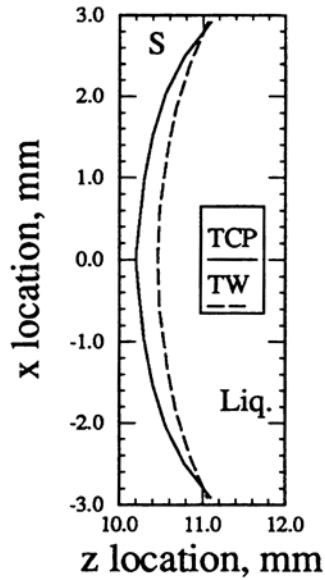


Figure 8. Top view of interface during melting, top-center-plane (x,2.5,z) and at the top wall of the ampoule (x,3,z).

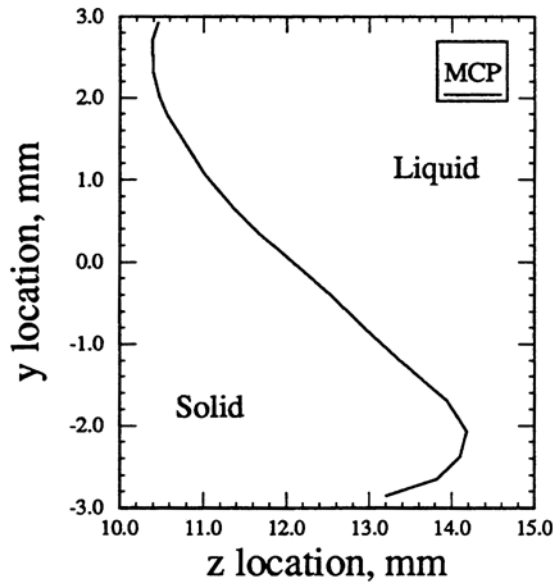


Figure 9. Side view of interface during melting, mid-center plane, y-z plane at x=0.

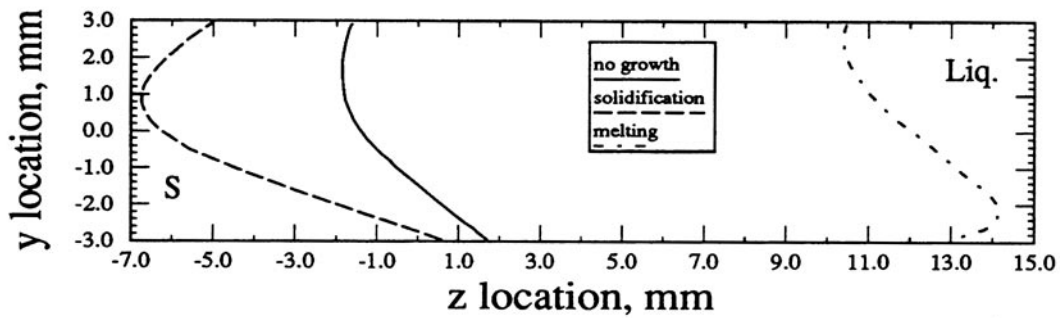


Figure 10. Comparison of side views of interfaces at the mid-center plane for no-growth, solidification, and melting cases.

## SUMMARY AND CONCLUSIONS

The objectives of this work were to determine quantitatively the SCN interface shapes during no-growth, solidification, and melting conditions and to measure reliably the thermal conditions which resulted in these interfaces. This was done with results being presented in Figures 3 through 10 and Tables A1 through A13. We believe that the ampoule temperature profiles measured are adequate for use as input boundary conditions for numerical simulation of the cases examined in this study; and that the interface shapes and SCN liquid temperature measurements made will provide a sufficient benchmark test for comparison to numerical results.

In the three cases examined (no-growth, solidification, and melting) the s/l interface, as viewed from the liquid, was concave in the upper half of the ampoule; this was due to the convecting flow which brought relatively warm liquid from the hot zone and rammed it against the upper half of the interface. This flow of warm liquid moving toward the interface along the top ampoule wall, with cooler liquid returning along the bottom wall, resulted in a dominating thermal gradient in the y-direction (with the top hotter) and interface asymmetry as viewed in the y-z plane. During solidification, as the longitudinal thermal gradient is moved along the ampoule in the +z direction, the s/l interface in contact with the ampoule was moved along with it; however, the inner regions of the solid must conduct the heat through the relatively low conducting SCN, causing the solid near the ampoule center to lag behind the outer edges. Thermal gradients in the x-y plane and concavity in the upper region of the interface were largest during solidification and smallest during melting. Due to the input of heat during melting, and the weaker and cooler flow in the lower half of the ampoule, the interface was convex in the lower region ( $y < 0$ ) during melting. We believe that the heat transferred by the convecting liquid and conduction through the solid dominates the interface shape, and that the release of latent heat has little influence on the thermal conditions in the neighborhood of the interface. The influence of latent heat will be examined numerically in a later paper.

In the three cases examined the interfaces formed at distinctly different longitudinal locations ranging from about  $z = -7$  mm during solidification to  $z = 14$  mm during melting (with a gap, or adiabatic zone length of 5 mm, with  $z = 0$  at the center of the gap). The shapes and locations of these interfaces may help with the development and validation of numerical codes. The relationship between interface shape and interface location in the adiabatic region is an important part of the art and science of Bridgman crystal growth. It is hoped that through numerical

simulations the interface shape can be optimized through manipulation of the thermal gradient and interface location in the adiabatic zone, both of which are controlled primarily by hot end zone set points.

## References

- 1) R.A. Brown, AICHE Journal, 1988, vol. 34, No. 6, pp. 881-911.
- 2) A. Rouzaud, J. Comera, P. Contamin, B. Angelier, F. Herbillon and J.J Favier, J. Crystal Growth, 1993, vol. 129, pp. 173-178.
- 3) C. Mennetrier, M.A. Chopra, and H.C. de Groh III, FED vol. 111, Forum on Microgravity Flows, 1991, Ed. by A. Hashemi, B.N. Antar, and I. Tanasawa, Book No. G00599-1991, pp. 5-10.
- 4) W.A. Arnold, D.A. Jacqmin, R.L. Gaug, and A. Chait, J. of Spacecraft and Rockets, 1991, vol. 28, No. 2, pp. 238-244.
- 5) R.J. Schaefer and S.R. Coriell, Metall. Trans A, 1984, vol. 15A, pp. 2109-2115.
- 6) P. Brunet, A. Katty, D. Schneider, A. Thomson-Carli, and R. Triboulet, Mat. Sci. and Eng., 1993, B16, pp. 44-47.
- 7) J.P. Fraser and D.J. Oakley, Trans. of ASME, 1957, vol. 79, p. 1185.
- 8) G.S. Cole and W.C Winegard, J. of the Inst. of Metals, 1964-65, vol. 93, p. 153.
- 9) Z. Xu, P. Ge, C. Huo, and Z. Zhu, J. of Crystal Growth, 1993, vol. 129, pp. 506-514
- 10) Y. Inatomi, H. Miyashita, E. Sato, K. Kuribayashi, K. Itonaga, and T. Motegi, J. of Crystal Growth, 1993, vol. 130, pp. 85-95.
- 11) G.H. Yeoh, G. de Vahl Davis, E. Leonardi, H.C. de Groh III, and M. Yao, in proceedings of the First International Conference on Transport Phenomena in Processing, S.I. Güçeri editor, 1993, pp. 98-109.
- 12) FIDAP User Manuals, Fluid Mechanics International, Inc., 500 Davis St., Suite 600, Evanston IL 60201, USA.
- 13) M.A. Chopra, Ph.D. Thesis, Rensselaer Polytechnic Institute, 1984.
- 14) M.E. Glicksman, R.J. Scheafer and J.D. Ayers, Metall. Trans. A, 1976, vol. 7A, Nov., pp. 1747-1759.
- 15) Y. S. Touloukian, R.W. Powell, C.Y. Ho and P.G. Klemens, "Thermophysical Properties of Matter," 1970, IFI/Plenum, vol. 2, pp. 922-932.
- 16) M. Yao and H.C. de Groh III, "Three-Dimensional Finite Element Method Simuladon of Bridgman Crystal Growth and Comparison with Experiments," to appear in Numerical Heat Transfer, Part A: Applications, Dec. 1993, Vol. 24, Issue 4.
- 17) M. Yao and H.C. de Groh m, "A Numerical and Experimental Investigation of Heat Transport and Fluid Flow in Directional Solidification of Succinonitrile," in progress.

Table A1 Temperature data for no-growth condition (SCN4). Temperatures of the outside surface of the ampoule at various x-y locations and along the z-axis: Z, are z locations of temperature measurements (mm), T are temperatures in °C. Subscripts refer to: t for the top wall, (0,3,z); b for the ampoule bottom, (0,-3,z); c for center, (0,0,z); tc for top corner, ( $\pm 3,3,z$ ); bc, bottom corner ( $\pm 3,-3,z$ ); r for rear ( $\pm 3,0,z$ ); ui for upper inner (0,1.54,z).

Z <sub>t</sub>	T <sub>t</sub>	Z <sub>b</sub>	T <sub>b</sub>	Z <sub>c</sub>	T <sub>c</sub>	Z <sub>tc</sub>	T <sub>tc</sub>	Z <sub>bc</sub>	T <sub>bc</sub>	Z <sub>r</sub>	T <sub>r</sub>	Z <sub>ui</sub>	T <sub>ui</sub>
27.0	73.7	27.1	70.0	27.4	71.2	41.4	74.8	41.8	73.6	44.7	74.4	44.5	74.6
25.0	73.5	25.1	69.5	25.4	70.8	37.4	74.6	37.8	72.9	40.7	73.9	40.5	74.4
23.0	73.3	23.1	69.0	23.4	70.4	33.4	74.2	33.8	72.2	36.7	73.4	36.5	74.1
21.0	73.0	21.1	68.5	21.4	69.9	29.4	73.9	29.8	71.5	32.7	73.0	32.5	73.8
19.0	72.8	19.1	67.9	19.4	69.5	27.4	73.7	27.8	71.1	28.7	72.3	28.5	73.4
17.0	72.7	17.1	67.4	17.4	69.1	25.4	73.4	25.8	70.6	26.7	71.9	26.5	73.1
16.0	72.5	16.1	67.0	16.4	68.8	23.4	73.2	23.8	70.1	24.7	71.6	24.5	72.8
15.0	72.4	15.1	66.7	15.4	68.6	21.4	72.9	21.8	69.6	22.7	71.2	22.5	72.6
14.0	72.2	14.1	66.3	14.4	68.3	19.4	72.6	19.8	69.1	20.7	70.8	20.5	72.3
13.0	72.1	13.1	66.0	13.4	68.1	18.4	72.4	18.8	68.8	19.7	70.5	19.5	72.0
12.0	71.8	12.1	65.7	12.4	67.8	17.4	72.3	17.8	68.6	18.7	70.3	18.5	71.9
11.0	71.7	11.1	65.3	11.4	67.6	16.4	72.1	16.8	68.3	17.7	70.1	17.5	71.7
10.0	71.4	10.1	64.9	10.4	67.3	15.4	71.9	15.8	67.9	16.7	69.8	16.5	71.5
9.0	71.3	9.1	64.4	9.4	67.0	14.4	71.8	14.8	67.7	15.7	69.5	15.5	71.2
8.0	70.9	8.1	63.8	8.4	66.7	13.4	71.4	13.8	67.4	14.7	69.3	14.5	71.2
7.0	70.7	7.1	63.4	7.4	66.5	12.4	71.2	12.8	67.0	13.7	69.2	13.5	71.1
6.0	70.2	6.1	62.6	6.4	66.2	11.4	71.1	11.8	66.8	12.7	69.0	12.5	71.0
5.0	69.8	5.1	61.8	5.4	66.0	10.4	71.0	10.8	66.4	11.7	68.8	11.5	70.9
4.0	68.9	4.1	60.8	4.4	65.7	9.4	70.8	9.8	66.1	10.7	68.4	10.5	70.6
3.0	68.1	3.1	59.6	3.4	65.5	8.4	70.7	8.8	65.8	9.7	68.2	9.5	70.5
2.0	66.5	2.1	57.9	2.4	65.4	7.4	70.3	7.8	65.2	8.7	67.9	8.5	70.2
1.0	64.0	1.1	55.0	1.4	65.4	6.4	70.0	6.8	64.7	7.7	67.6	7.5	70.1
0.0	61.0	0.1	52.1	0.4	64.6	5.4	69.5	5.8	64.0	6.7	67.1	6.5	69.8
-0.6	59.8	-0.5	51.5	-0.2	63.9	4.4	69.0	4.8	63.3	5.7	66.8	5.5	69.7
-1.0	57.6	-0.9	50.3	-0.6	61.2	3.4	68.1	3.8	62.1	4.7	66.2	4.5	69.4
-2.0	52.6	-1.9	47.0	-1.6	56.1	2.4	67.1	2.8	60.9	3.7	65.6	3.5	69.2
-3.0	47.7	-2.9	43.9	-2.6	50.3	1.4	65.3	1.8	59.0	2.7	64.0	2.5	68.6
-4.0	43.4	-3.9	41.1	-3.6	45.7	0.4	63.5	0.8	57.1	1.7	62.6	1.5	68.3
-5.0	39.8	-4.9	38.3	-4.6	41.7	0.1	62.2	0.5	55.8	0.7	60.3	0.5	67.8
-6.0	37.2	-5.9	36.3	-5.6	38.9	-0.6	59.0	-0.2	53.1	0.3	59.4	0.1	67.6
-7.0	33.5	-6.9	33.3	-6.6	35.2	-1.6	56.1	-1.2	50.8	-0.3	58.0	-0.5	67.5
-8.0	31.8	-7.9	31.8	-7.6	33.4	-2.6	50.8	-2.2	47.0	-1.3	53.3	-1.5	62.5
-9.0	29.3	-8.9	29.5	-8.6	30.7	-3.6	47.2	-3.2	44.3	-2.3	49.8	-2.5	54.3
-10.0	27.9	-9.9	28.2	-9.6	29.2	-4.6	41.8	-4.2	40.3	-3.3	45.1	-3.5	46.3
-11.0	26.0	-10.9	26.4	-10.6	27.2	-5.6	38.8	-5.2	37.8	-4.3	41.1	-4.5	41.1
-12.0	24.9	-11.9	25.3	-11.6	26.0	-6.6	34.9	-6.2	34.5	-5.3	38.6	-5.5	38.3
-13.0	23.5	-12.9	23.8	-12.6	24.4	-7.6	31.8	-7.2	31.7	-6.3	35.3	-6.5	34.8

A1 continued

-14.0	23.0	-13.9	23.3	-13.6	23.8	-8.6	30.3	-8.2	30.3	-7.3	33.1	-7.5	32.5
-15.0	21.0	-14.9	21.3	-14.6	21.8	-9.6	27.9	-9.2	28.1	-8.3	30.7	-8.5	30.0
-16.0	20.9	-15.9	21.2	-15.6	21.6	-10.6	26.5	-10.2	26.7	-9.3	28.8	-9.5	28.2
-17.0	19.6	-16.9	20.0	-16.6	20.3	-11.6	24.8	-11.2	25.0	-10.3	26.7	-10.5	26.1
-18.0	19.5	-17.9	19.8	-17.6	20.1	-12.6	23.6	-12.2	23.9	-11.3	25.6	-11.5	25.0
-19.0	18.2	-18.9	18.5	-18.6	18.7	-13.6	22.2	-13.2	22.4	-12.3	23.8	-12.5	23.3
-21.0	17.0	-20.9	17.2	-20.6	17.4	-14.6	21.5	-14.2	21.8	-13.3	23.2	-13.5	22.7
-23.0	16.1	-22.9	16.3	-22.6	16.5	-15.6	20.2	-15.2	20.4	-14.3	21.4	-14.5	20.9
-25.0	15.5	-24.9	15.6	-24.6	15.8	-16.6	20.0	-16.2	20.2	-15.3	21.0	-15.5	20.6
-29.0	14.8	-28.9	14.9	-28.6	15.0	-18.6	18.5	-18.2	18.6	-16.3	19.8	-16.5	19.4
-29.0	14.8	-28.9	14.9	-28.6	15.0	-21.6	16.3	-21.2	16.4	-18.3	18.2	-18.5	17.9
-29.0	14.8	-28.9	14.9	-28.6	15.0	-23.6	15.5	-23.2	15.6	-20.3	16.9	-20.5	16.7

Table A2 Temperature data during solidification (SCN8). Temperatures of the outside surface of the ampoule at various x,y locations and along the z axis: Z, are z locations of temperature measurements in mm, T are temperatures in °C. Subscripts refer to: tc for top corner, ( $\pm 3, 3, z$ ); bc, bottom corner ( $\pm 3, -3, z$ ); t for the top wall, ( $0, 3, z$ ); b for the ampoule bottom, ( $0, -3, z$ ); r for rear ( $\pm 3, 0, z$ ).

Z <sub>tc</sub>	T <sub>tc</sub>	Z <sub>bc</sub>	T <sub>bc</sub>	Z <sub>t</sub>	T <sub>t</sub>	Z <sub>b</sub>	T <sub>b</sub>	Z <sub>r</sub>	T <sub>r</sub>
31.4	71.68	31.6	70.09	44.0	72.74	43.9	71.70	26.5	69.94
29.4	71.60	29.6	69.97	42.0	72.71	41.9	71.70	24.5	69.82
27.6	71.53	27.8	69.75	40.2	72.69	40.1	71.56	22.7	69.58
24.7	71.27	24.9	69.12	37.3	72.64	37.2	71.12	19.8	69.12
21.9	70.88	22.1	68.38	34.5	72.52	34.4	70.54	17.0	68.40
19.0	70.45	19.2	67.56	31.6	72.28	31.5	69.85	14.1	67.71
16.4	70.06	16.6	66.84	29.0	72.04	28.9	69.25	11.5	67.06
15.4	69.87	15.6	66.46	28.0	71.94	27.9	68.96	10.5	66.77
14.4	69.73	14.6	66.22	27.0	71.87	26.9	68.76	9.5	66.50
12.6	69.37	12.8	65.59	25.2	71.65	25.1	68.23	7.7	65.88
11.6	69.20	11.8	65.33	24.2	71.56	24.1	68.02	6.7	65.59
10.6	68.98	10.8	64.92	23.2	71.44	23.1	67.73	5.7	65.09
9.7	68.81	9.9	64.63	22.3	71.34	22.2	67.47	4.8	64.65
8.7	68.57	8.9	64.20	21.3	71.19	21.2	67.18	3.8	64.03
7.7	68.35	7.9	63.86	20.3	71.12	20.2	66.94	2.8	63.33
6.7	68.02	6.9	63.24	19.3	70.98	19.2	66.65	1.8	62.18
5.8	67.75	6.0	62.78	18.4	70.88	18.3	66.38	0.9	61.22
4.9	67.42	5.1	62.32	17.5	70.79	17.4	66.14	-0.04	59.88
3.6	66.70	3.8	61.15	16.2	70.62	16.1	65.76	-1.3	57.87
2.6	65.95	2.8	60.31	15.2	70.50	15.1	65.42	-2.3	55.95
1.6	64.75	1.8	58.87	14.2	70.35	14.1	65.09	-3.3	53.87
0.7	63.74	0.9	57.84	13.3	70.23	13.2	64.80	-4.2	52.29
-0.3	62.01	-0.08	56.62	12.3	70.11	12.2	64.44	-5.2	50.28

A2 continued

-1.2	60.72	-1.0	55.57	11.4	69.99	11.3	64.15	-6.1	48.39
-2.1	59.26	-1.9	54.37	10.5	69.85	10.4	63.81	-7.0	46.39
-3.6	56.98	-3.4	52.41	9.0	69.63	8.9	63.28	-8.5	42.89
-4.3	55.21	-4.1	50.81	8.3	69.43	8.2	62.92	-9.2	40.48
-5.5	53.58	-5.3	49.47	7.1	69.29	7.0	62.64	-10.4	38.61
-6.5	51.14	-6.3	47.55	6.1	69.05	6.0	62.11	-11.4	36.37
-7.5	48.54	-7.3	45.95	5.1	68.84	5.0	61.61	-12.4	34.75
-8.4	46.89	-8.2	44.30	4.2	68.57	4.1	61.08	-13.3	33.15
-9.4	43.71	-9.2	41.88	3.2	68.02	3.1	60.24	-14.3	31.23
-10.3	41.59	-10.1	40.21	2.3	67.49	2.2	59.57	-15.2	30.00
-11.3	39.05	-11.1	38.14	1.3	66.60	1.2	58.54	-16.2	28.53
-12.4	36.64	-12.2	36.08	0.2	65.35	0.1	57.55	-17.3	27.15
-13.5	34.60	-13.3	34.23	-0.9	63.89	-1.0	56.84	-18.4	25.97
-14.4	33.03	-14.2	32.81	-1.8	62.66	-1.9	55.66	-19.3	25.05
-15.5	31.18	-15.3	31.09	-2.9	60.91	-3.0	54.32	-20.4	23.97
-16.5	29.61	-16.3	29.61	-3.9	59.40	-4.0	52.86	-21.4	23.03
-17.6	28.23	-17.4	28.21	-5.0	58.03	-5.1	51.22	-22.5	22.17
-18.6	26.85	-18.4	26.90	-6.0	56.31	-6.1	49.57	-23.5	21.33
-19.7	25.67	-19.5	25.72	-7.1	54.13	-7.2	47.80	-24.6	20.62
-20.5	24.78	-20.3	24.83	-7.9	51.96	-8.0	46.32	-25.4	20.05
-21.6	23.75	-21.4	23.80	-8.9	48.95	-9.0	44.32	-26.4	19.38
-22.5	22.96	-22.3	23.03	-9.9	46.44	-10.0	42.75	-27.4	18.91
-24.4	21.28	-24.2	21.36	-11.8	40.75	-11.9	38.93	-29.3	17.85
-26.4	19.97	-26.2	20.07	-13.8	36.42	-13.9	35.68	-31.3	17.03
-28.5	18.71	-28.3	18.79	-15.9	32.36	-16.0	32.36	-33.4	16.19
-30.5	17.58	-30.3	17.72	-17.9	28.97	-18.0	29.49	-35.4	15.50
-31.5	17.10	-31.3	17.20	-18.9	27.52	-19.0	28.16	-36.4	15.17

Table A3 Temperature data during melting (SCN9). Temperatures of the outside surface of the ampoule at various x,y locations and along the z axis: Z, are z locations of temperature measurements in mm, T are temperatures in °C. Subscripts refer to: tc for top corner, ( $\pm 3, 3, z$ ); bc, bottom corner ( $\pm 3, -3, z$ ); t for the top wall, ( $0, 3, z$ ); b for the ampoule bottom, ( $0, -3, z$ ); r for rear ( $\pm 3, 0, z$ ).

Z <sub>tc</sub>	T <sub>tc</sub>	Z <sub>bc</sub>	T <sub>bc</sub>	Z <sub>t</sub>	T <sub>t</sub>	Z <sub>b</sub>	T <sub>b</sub>	Z <sub>r</sub>	T <sub>r</sub>
-34.8	13.49	-34.7	13.31	-22.2	15.79	-22.3	15.35	-39.8	13.14
-32.7	12.91	-32.6	12.79	-20.1	15.10	-20.2	14.75	-37.7	12.64
-30.9	12.57	-30.8	12.47	-18.3	14.65	-18.4	14.38	-35.9	12.32
-28.8	12.29	-28.7	12.19	-16.2	14.33	-16.3	14.06	-33.8	12.05
-26.8	12.05	-26.7	12.00	-14.2	14.18	-14.3	13.98	-31.8	11.85
-25.8	11.97	-25.7	11.92	-13.2	14.21	-14.3	14.01	-30.8	11.77
-24.7	11.92	-24.6	11.85	-12.1	14.30	-12.2	14.11	-29.7	11.70
-23.7	11.85	-23.6	11.77	-11.1	14.48	-11.2	14.28	-28.7	11.62
-22.8	11.82	-22.7	11.75	-10.2	14.68	-10.3	14.50	-27.8	11.60

A3 continued

-21.7	11.80	-21.6	11.70	-9.1	15.10	-9.2	14.90	-26.7	11.55
-20.9	11.75	-20.8	11.72	-8.3	15.57	-8.4	15.32	-25.9	11.52
-19.8	11.75	-19.7	11.72	-7.2	16.29	-7.3	16.04	-24.8	11.50
-18.9	11.75	-18.8	11.72	-6.3	16.98	-6.4	16.73	-23.9	11.47
-17.9	11.80	-17.8	11.75	-5.3	18.17	-5.4	17.92	-22.9	11.45
-16.9	11.85	-16.8	11.77	-4.3	19.23	-4.4	19.06	-21.9	11.47
-16.0	11.92	-15.9	11.87	-3.4	20.91	-3.5	20.89	-21.0	11.47
-15.1	12.02	-15.0	11.95	-2.5	22.49	-2.6	22.66	-20.1	11.50
-14.1	12.17	-14.0	12.07	-1.5	24.83	-1.6	25.55	-19.1	11.50
-13.2	12.32	-13.1	12.22	-0.6	27.00	-0.7	28.18	-18.2	11.55
-12.2	12.54	-12.1	12.44	0.4	29.98	0.3	31.80	-17.2	11.60
-11.2	12.77	-11.1	12.69	1.4	32.56	1.3	34.60	-16.2	11.67
-10.2	13.14	-10.1	13.06	2.4	36.05	2.3	39.15	-15.2	11.77
-9.3	13.51	-9.2	13.41	3.3	38.78	3.2	42.40	-14.3	11.90
-8.3	14.06	-8.2	13.96	4.3	42.03	4.2	45.70	-13.3	12.05
-7.4	14.63	-7.3	14.50	5.2	44.55	5.1	48.02	-12.4	12.22
-6.4	15.45	-6.3	15.35	6.2	47.48	6.1	50.55	-11.4	12.52
-5.5	16.26	-5.4	16.16	7.1	49.69	7.0	52.36	-10.5	12.79
-4.5	17.55	-4.4	17.48	8.1	52.41	8.0	54.39	-9.5	13.21
-3.6	18.79	-3.5	18.66	9.0	54.49	8.9	55.78	-8.6	13.63
-2.6	20.66	-2.5	20.66	10.0	57.17	9.9	57.27	-7.6	14.26
-1.7	22.49	-1.6	22.64	10.9	59.47	10.8	58.27	-6.7	14.88
-0.6	25.28	-0.5	25.67	12.0	62.54	11.9	59.38	-5.6	15.87
0.2	27.71	0.3	28.23	12.8	64.44	12.7	60.19	-4.8	16.81
1.3	31.06	1.4	32.04	13.9	66.10	13.8	61.20	-3.7	18.22
2.3	34.65	2.4	35.93	14.9	67.13	14.8	62.06	-2.7	19.97
3.3	38.32	3.4	39.89	15.9	67.83	15.8	62.88	-1.7	22.22
4.2	41.12	4.3	42.75	16.8	68.23	16.7	63.40	-0.8	24.32
5.3	44.30	5.4	45.90	17.9	68.62	17.8	64.01	0.3	27.27
6.1	46.59	6.2	48.15	18.7	68.86	18.6	64.44	1.1	29.83
7.2	49.28	7.3	50.64	19.8	69.10	19.7	64.87	2.2	33.35
8.1	51.26	8.2	52.39	20.7	69.27	20.6	65.18	3.1	36.03
9.1	53.58	9.2	54.39	21.7	69.44	21.6	65.57	4.1	39.42
10.0	55.38	10.1	55.78	22.6	69.58	22.5	65.83	5.0	41.91
11.0	57.65	11.1	57.31	23.6	69.73	23.5	66.17	6.0	45.01
11.9	59.57	12.0	58.37	24.5	69.82	24.4	66.38	6.9	47.26
13.9	63.96	14.0	60.86	26.5	70.06	26.4	66.91	8.9	51.98
15.8	66.24	15.9	62.71	28.4	70.28	28.3	67.34	10.8	55.62
17.6	67.49	17.7	64.10	30.2	70.45	30.1	67.75	12.6	59.06
19.7	68.23	19.8	65.18	32.3	70.67	32.2	68.21	14.7	62.64
21.7	68.76	21.8	65.97	34.3	70.86	34.2	68.64	16.7	64.63
23.8	69.15	23.9	66.58	36.4	71.03	36.3	69.05	18.8	65.73
25.6	69.44	25.7	67.03	38.2	71.17	38.1	69.39	20.6	66.38
27.3	69.68	27.4	67.51	39.7	71.29	39.6	69.68	22.3	66.84

---

Table A4 Interface shape for no-growth case, top-center-plane, (x,z) data in mm at y=1.54mm. See Figure 4.

---

z	x
-0.857	-2.940
-1.147	-2.710
-1.467	-2.305
-1.625	-2.030
-1.867	-1.490
-2.023	-0.930
-2.111	-0.320
-2.129	-0.112
-2.129	0.112
-2.111	0.320
-2.023	0.930
-1.867	1.490
-1.625	2.030
-1.467	2.305
-1.147	2.710
-0.857	2.94

---

---

Table A5 Interface shape for no-growth case, top wall, (x,z) data in mm at y=3mm. See Figure 4.

---

z	x
-0.761	-2.930
-0.914	-2.570
-1.001	-2.380
-1.217	-1.760
-1.291	-1.520
-1.391	-1.073
-1.440	-0.580
-1.452	-0.325
-1.454	-0.216
-1.454	0.216
-1.452	0.325
-1.440	0.580
-1.391	1.073
-1.291	1.520
-1.217	1.760
-1.001	2.380
-0.914	2.570
-0.761	2.930

---

---

Table A6 Interface shape for no-growth case, mid-center-plane, (y,z) data in mm at  $x=0$ . See Figure 5.

---

z	y
-1.610	2.922
-1.657	2.873
-1.700	2.755
-1.736	2.612
-1.763	2.506
-1.794	2.360
-1.816	2.229
-1.844	2.067
-1.866	1.886
-1.861	1.715
-1.862	1.518
-1.854	1.319
-1.825	1.082
-1.793	0.850
-1.686	0.552
-1.581	0.300
-1.425	0.045
-1.261	-0.199
-1.051	-0.436
-0.871	-0.634
-0.684	-0.797
-0.510	-0.997
-0.260	-1.226
0.014	-1.478
0.224	-1.673
0.516	-1.944
0.828	-2.213
1.137	-2.483
1.354	-2.643
1.500	-2.790
1.645	-2.905
1.705	-2.945

---

---

Table A7 Interface shape for no-growth case, front wall, (y,z) data in mm at x=3mm. See Figure 5.

---

z	x
-0.879	2.943
-0.810	2.892
-0.743	2.817
-0.682	2.726
-0.641	2.625
-0.618	2.502
-0.620	2.359
-0.628	2.203
-0.645	2.051
-0.641	1.871
-0.619	1.659
-0.606	1.483
-0.565	1.278
-0.519	1.125
-0.467	0.947
-0.396	0.761
-0.305	0.558
-0.228	0.377
-0.155	0.232
-0.090	0.065
-0.023	-0.079
0.047	-0.221
0.140	-0.385
0.218	-0.536
0.298	-0.698
0.392	-0.902
0.520	-1.135
0.622	-1.273
0.720	-1.410
0.812	-1.564
0.956	-1.769
1.038	-1.920
1.140	-2.082
1.234	-2.237
1.355	-2.415
1.452	-2.541
1.550	-2.688
1.626	-2.804
1.694	-2.920
1.721	-2.945

---

---

Table A8 Interface shape during solidification, top-center-plane, (x,z) data in mm at y=1.mm. See Figure 6.

---

x	z
-2.897	-3.6
-2.88	-3.68
-2.806	-3.92
-2.526	-4.46
-2.277	-4.85
-1.9	-5.36
-1.64	-5.66
-1.314	-6.03
-.891	-6.39
-.598	-6.57
-.305	-6.65
-.11	-6.67
-.02	-6.681
.02	-6.681
.11	-6.67
.305	-6.65
.598	-6.57
.891	-6.39
1.314	-6.03
1.64	-5.66
1.9	-5.36
2.277	-4.85
2.526	-4.46
2.806	-3.92
2.88	-3.68
2.897	-3.6

---

---

Table A9 Interface shape during solidification, top wall, (x,z) data in mm at y=3mm. See Figure 6.

---

x	z
-2.863	-3.49
-2.826	-3.51
-2.7	-3.62
-2.58	-3.72
-2.217	-4.02
-1.98	-4.21
-1.647	-4.47
-1.21	-4.72
-1.1	-4.77
-.868	-4.85
-.553	-4.93
-.326	-4.96
-.133	-4.97
-.035	-4.97
.035	-4.97
.133	-4.97
.326	-4.96
.553	-4.93
.868	-4.85
1.1	-4.77
1.21	-4.72
1.647	-4.47
1.98	-4.21
2.217	-4.02
2.58	-3.72
2.7	-3.62
2.826	-3.51
2.863	-3.49

---

---

Table A10 Interface shape during solidification, mid-center-plane, (y,z) data in mm at x=0. See Figure 7.

---

z	x
.58	-2.95
-.62	-2.5
-1.97	-2.01
-3.23	-1.52
-4.4	-1.03
-5.56	-.5
-6.28	.018
-6.5	.25
-6.66	.51
-6.74	.765
-6.74	1.01
-6.67	1.26
-6.52	1.52
-6.33	1.76
-6.12	2.
-5.6	2.5
-5.04	2.93

---

---

Table A11 Interface shape during melting (SCN9), top-center-plane, (x,z) data in mm at y=2.5mm. See Figure 8.

---

z	x
11.10	2.92
10.78	2.50
10.55	2.03
10.40	1.53
10.30	1.00
10.20	.09
10.20	-.09
10.30	-1.00
10.40	-1.53
10.55	-2.03
10.78	-2.50
11.10	-2.92

---

---

Table A12 Interface shape during melting (SCN9), top wall, (x,z) data in mm at y=3mm. See Figure 8.

---

z	x
11.06	2.92
10.84	2.39
10.68	1.86
10.58	1.35
10.48	.61
10.46	.06
10.46	-.06
10.48	-.61
10.58	-1.35
10.68	-1.86
10.84	-2.39
11.06	-2.92

---

---

Table A13 Interface shape during melting (SCN9), mid-center-plane, (y,z) data in mm at x=0. See Figure 8.

---

z	y
10.46	2.93
10.39	2.71
10.40	2.31
10.47	2.02
10.56	1.80
11.01	1.076
11.36	.657
11.66	.354
11.94	.12
12.52	-.39
12.97	-.83
13.37	-1.20
13.94	-1.696
14.18	-2.07
14.10	-2.38
13.82	-2.65
13.20	-2.854

---

# REPORT DOCUMENTATION PAGE

*Form Approved*  
OMB No. 0704-0188

Public reporting burden for this collection of information is estimated to average 1 hour per response, including the time for reviewing instructions, searching existing data sources, gathering and maintaining the data needed, and completing and reviewing the collection of information. Send comments regarding this burden estimate or any other aspect of this collection of information, including suggestions for reducing this burden, to Washington Headquarters Services, Directorate for Information Operations and Reports, 1215 Jefferson Davis Highway, Suite 1204, Arlington, VA 22202-4302, and to the Office of Management and Budget, Paperwork Reduction Project (0704-0188), Washington, DC 20503.

<b>1. AGENCY USE ONLY</b> ( <i>Leave blank</i> )		<b>2. REPORT DATE</b> June 1994	<b>3. REPORT TYPE AND DATES COVERED</b> Technical Memorandum	
<b>4. TITLE AND SUBTITLE</b> Interface Shape and Convection During Solidification and Melting of Succinonitrile			<b>5. FUNDING NUMBERS</b>  WU-674-21-05	
<b>6. AUTHOR(S)</b>  Henry C. de Groh III and Tiffany Lindstrom				
<b>7. PERFORMING ORGANIZATION NAME(S) AND ADDRESS(ES)</b>  National Aeronautics and Space Administration Lewis Research Center Cleveland, Ohio 44135-3191			<b>8. PERFORMING ORGANIZATION REPORT NUMBER</b>  E-8474	
<b>9. SPONSORING/MONITORING AGENCY NAME(S) AND ADDRESS(ES)</b>  National Aeronautics and Space Administration Washington, D.C. 20546-0001			<b>10. SPONSORING/MONITORING AGENCY REPORT NUMBER</b>  NASA TM-106487	
<b>11. SUPPLEMENTARY NOTES</b> Henry C. de Groh III, NASA Lewis Research Center, and Tiffany Lindstrom, University of Arizona, Department of Materials Science and Engineering, Tucson, Arizona, 85721 (work funded by NASA Grant NAG3-1446). Responsible person, Henry C. de Groh III, organization code 5110, (216) 433-5025.				
<b>12a. DISTRIBUTION/AVAILABILITY STATEMENT</b>  Unclassified - Unlimited Subject Category 34			<b>12b. DISTRIBUTION CODE</b>	
<b>13. ABSTRACT</b> ( <i>Maximum 200 words</i> )  An experimental study was conducted of the crystal growth of succinonitrile during solidification, melting and no-growth conditions using a horizontal Bridgman furnace and square glass ampoule. For use as input boundary conditions to numerical codes, thermal profiles on the outside of the ampoule at five locations around its periphery were measured along the ampoule's length. Temperatures inside the ampoule were also measured. The shapes of the s/l interface in various two-dimensional planes were quantitatively determined. Though interfaces were nondendritic and noncellular, they were not flat, but were highly curved and symmetric in only one unique longitudinal y-z plane (at x=0). The shapes of the interface were dominated by the primary longitudinal flow cell characteristic of shallow cavity flow in horizontal Bridgman; this flow cell was driven by the imposed furnace temperature gradient and caused a "radical" thermal gradient such that the upper half of the ampoule was hotter than the bottom half. We believe that due to the strong convection, the release of latent heat does not significantly influence the thermal conditions near the interface. We hope that the interface shape and thermal data presented in this paper can be used to optimize crystal growth processes and validate numerical models.				
<b>14. SUBJECT TERMS</b>  Convection; Solidification; Succinonitrile; Melting; Bridgman			<b>15. NUMBER OF PAGES</b> 24	
			<b>16. PRICE CODE</b> A03	
<b>17. SECURITY CLASSIFICATION OF REPORT</b> Unclassified	<b>18. SECURITY CLASSIFICATION OF THIS PAGE</b> Unclassified	<b>19. SECURITY CLASSIFICATION OF ABSTRACT</b> Unclassified	<b>20. LIMITATION OF ABSTRACT</b>	